International Journal of Heat and Mass Transfer 227 (2024) 125497

Contents lists available at ScienceDirect

International Journal of Heat and Mass Transfer

journal homepage: www.elsevier.com/locate/ijhmt

Experimental and numerical simulation study of a novel double shell-passes multi-layer helically coiled tubes heat exchanger

Yuyang Yuan, Jiaming Cao, Zhao Zhang, Zhengyan Xiao, Xuesheng Wang *

Key Laboratory of Pressure System and Safety, Ministry of Education, East China University of Science and Technology, Shanghai 200237, China

ARTICLE INFO

Keywords:
Helically coiled tubes
Heat exchangers
Heat transfer enhancement
Numerical simulation
Experimental study

ABSTRACT

To enhance the heat transfer efficiency of the helically coiled tubes heat exchangers, this paper proposes a double shell-passes structure designed for a multi-layer helically coiled tubes heat exchanger. Numerical simulation is employed to investigate the performance of the Double Shell-passes Multi-layer Helically Coiled Tubes Heat Exchanger (DSMHCTHE). Furthermore, an experimental test system is constructed to validate the simulation results, exploring the performance under different operating conditions. A comparative analysis is conducted with the traditional Multi-Layer Helical Tube Heat Exchanger (MHCTHE). The results indicate that, under identical experimental conditions, the heat transfer rate and thermal effectiveness of DSMHCTHE increased by 5.1 % to 12.9 %. The overall heat transfer coefficient showed an improvement ranging from 21.5 % to 29.0 %, while the shell-side heat transfer coefficient increased by 36.2 % to 47.5 %. However, the shell-side pressure drop increased by 60.7 % to 83.4 %. Utilizing the heat exchanger's comprehensive performance as the evaluation criterion, it was observed that DSMHCTHE exhibited superior comprehensive performance. In comparison to MHCTHE, the comprehensive performance of DSMHCTHE improved by 12 %. The design of the double shell-passes configuration has shown significant enhancements in both convective heat transfer and overall performance, highlighting the superior application potential of DSMHCTHE.

1. Introduction

Helically coiled tubes heat exchangers have advantages such as compact structure, low pressure loss, and high heat transfer coefficient [1,2]. Secondary flow occurs in the plane perpendicular to the main flow direction inside the helically coiled tubes, which is one of the important reasons for enhancing the flow and heat transfer performance in the helically coiled tubes. Compared to conventional straight tubes heat exchangers, helical structure occupies less space, has a larger heat transfer surface area per unit volume, and is widely applicable. Due to the various advantages, helically coiled tubes heat exchangers have been widely applied in industries such as power generation, petrochemicals, food industry, heating ventilation and air conditioning(HVAC), and waste heat recovery systems [3,4].

The structure of the helically coiled tube heat exchanger is shown in Fig. 1. Due to the helical structure, the critical Reynolds number for the transition from laminar to turbulent flow inside the coil is higher than that of a straight tube [5]. Ito [6] conducted relevant research on the calculation of the critical Reynolds number inside the helically coiled tubes, and obtained correlations for heat transfer and resistance inside the tubes.

Some scholars have studied the overall performance of helical coil heat exchangers through experimental testing or numerical simulation methods. Salimpour et al. [7,8]. conducted experimental studies on single-layer helical coil heat exchangers with three different coil pitches and curvatures. They analyzed the variation of the shell-side heat transfer coefficient using the wilson plot method and found that helical coils with larger pitches can increase the shell-side heat transfer coefficient. Jamshidi et al. [9]. experimentally tested the influence of flow rate, helically coiled diameters, and coil pitches on the performance of a single-layer helical coil heat exchanger. By using the Taguchi method [10], they obtained the optimal operating parameters within the experimental conditions. Majid Etghani [11] designed samples using the Taguchi method, calculated the exergy loss of a single-layer helically coiled tube heat exchangers through numerical simulation, and obtained optimized structural parameters. Ghorbani et al. [12,13]. constructed helically coiled tube heat exchanger with different helically coiled diameters and pitches. They evaluated the effects of geometric parameters of the helical coil and changes in tube-side flow rate on the shell-side heat transfer coefficient and overall heat transfer performance of the heat exchanger under laminar and turbulent flow conditions inside the coil. They also introduced the concept of 'equivalent shell diameter' and

* Corresponding author.
E-mail address: wangxs@ecust.edu.cn (X. Wang).

https://doi.org/10.1016/j.ijheatmasstransfer.2024.125497
Received 4 February 2024; Received in revised form 10 March 2024; Accepted 25 March 2024
Available online 9 April 2024
0017-9310/© 2024 Elsevier Ltd. All rights reserved.

Nomenclature

A	The area of heat transfer (m^2)
c_p	Specific heat capacity ($J \bullet kg^{-1} \bullet K^{-1}$)
D	Coil diameter (m)
D_1	Inner tube coil diameter (m)
D_2	Outer tube coil diameter (m)
D_{Core1}	Diameter of inner guide cylinder (m)
D_{Core2}	Diameter of outer guide cylinder (m)
D_h	Hydraulic diameter (m)
d_i	Internal diameter of tubes (m)
d_o	External diameter of tubes (m)
h	Heat transfer coefficient ($W\ m^{-2}\ K^{-1}$)
H	Coil pitch (m)
H_1	Inner tube coil pitch (m)
H_2	Outer tube coil pitch (m)
He	Helical number (-) ($He = Re\sqrt{d/D}/\sqrt{1+(H/\pi D)^2}$)
L	Length (m)
m	flow rate ($kg\ s^{-1}$)
Nu	Nusselt number (-)
ΔP	Pressure drop (Pa)
Pr	Prandtl number (-)
Q	Heat transfer rate (W)
Re	Reynolds number (-)
Re_{cr}	Critical Reynolds number (-)
T	Temperature (K)
$\overline{T}$	Average temperature (K)
ΔT_{LMTD}	Logarithmic mean temperature difference (K)
u	Velocity component ($m\ s^{-1}$)
U_o	Overall heat transfer coefficient ($W\ m^{-2}\ K^{-1}$)
V	Space volume (m^3)
W_P	Pump power (W)

Greek symbols

ε	Thermal effectiveness (-)
λ	Thermal conductivity ($W\ m^{-1}\ K^{-1}$)
μ	Dynamic viscosity (Pa s)
ξ	Comprehensive performance (-)
ρ	Density ($kg\ m^{-3}$)

Subscript

S	Shell-side
Si	Shell-side inlet
So	Shell-side outlet
T	Tube-side
Ti	Tube-side inlet
To	Tube-side outlet
w	Wall

Abreviation

MHCTHE	Multi-layer helically coiled tubes heat exchangers
DSMHCTHE	Double shell-passes multi-layer helically coiled tubes heat exchanger

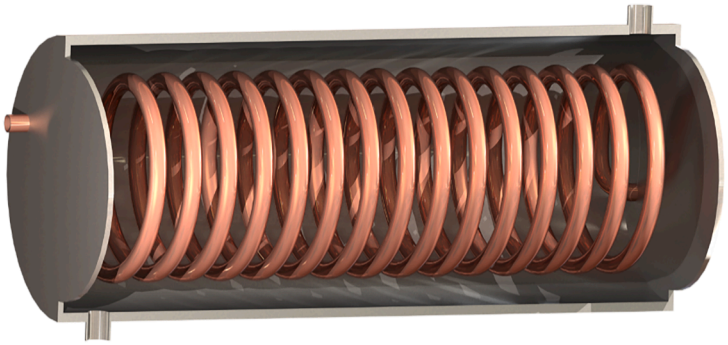

Fig. 1. Diagram of the helicallyly coiled tube heat exchanger structure.

experimentally demonstrated its effectiveness.

Some studies have sought to enhance heat transfer on the side of helically coiled tube to improve the heat transfer performance of the heat exchangers. There are currently two mainstream methods: one involves improving the heat transfer surface of the tubes, disrupting the heat transfer inflation layer, and enhancing heat transfer efficiency; the other involves using nanofluids as the flowing medium, which enhances fluid mixing pulsation and turbulence. Yuan et al. [14]. proposed an internally finned helically coiled tube and conducted numerical simulations to investigate its flow and heat transfer characteristics. The comprehensive performance of the finned tube increased by 40 % compared to that of a conventional smooth helically coiled tube. Kurnia et al. [15]. investigated the heat transfer performance and entropy generation of helically coiled tubes with circular, elliptical, and square cross-sections. The results indicated that the square cross-section tubes exhibited the best heat transfer performance. Omidi et al. [16]. introduced a lobed cross-section helically coiled tubes, and numerical simulations revealed that higher numbers of lobed led to better overall performance. Zheng et al. [17]. incorporated shallow groove structures on the helically coiled tubes wall, and numerical simulations demonstrated that this structure could increase the Nusselt number by up to 2 times. Chang et al. [18]. proposed a square-twisted helically coiled tubes, which showed a 19 % enhancement in heat transfer coefficient and a 69.8 % increase in pressure drop compared to the smooth square helically coiled tubes. Wang et al. [19]. conducted numerical simulations on helically coiled tubes with elliptical and trilobate cross-sections, concluding that the trilobate helically coiled tubes exhibited the best overall performance. Kumar et al. [20]. introduced a micro-finned helical tube, showing that when the number of fins reached 12, the Nusselt number increased by 51 % and the pressure drop increased by 36 %. Barzegari et al. [21]. experimentally investigated the flow and heat transfer performance of alumina nanofluid inside helically coiled tubes. The results indicated that higher heat transfer efficiency was achieved at lower concentrations of the nanofluid. Niwalkar et al. [22]. conducted experiments on the flow and heat transfer performance of water-based SiO_2 nanofluids with different volume fractions inside helically coiled tubes. The results showed that the heat transfer coefficient increased with increasing mass flow rate and nano volume fraction, and the heat

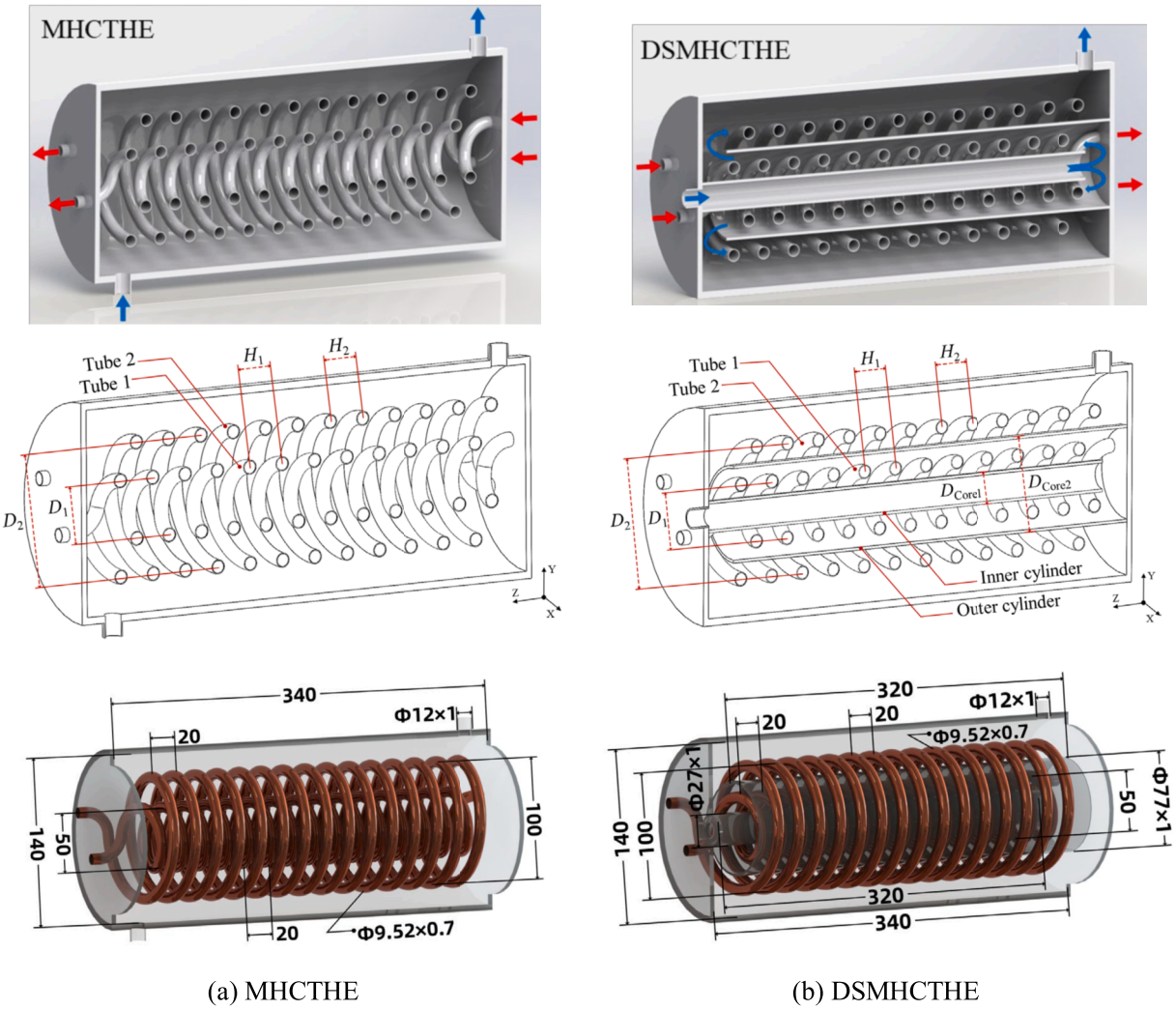

Fig. 2. The physical models of MHCTHE and DSMHCTHE.

transfer coefficient was 29 % higher and the pressure drop was 62 % higher compared to that of water as the fluid. Zaboli et al. [23]. numerically simulated the flow and heat transfer performance of Al_2O_3, CuO, and SiO_2 nanofluids with water as the base fluid inside helically coiled tubes. The results indicated that CuO nanofluid exhibited the best heat transfer performance.

The shell-side convective heat transfer coefficient of a helically coiled tubes heat exchanger is typically lower than the convective heat transfer coefficient inside the coil, which may lead to a reduction in the overall heat transfer efficiency of the heat exchanger. In response to the above issue, some scholars have also conducted research on enhanced heat transfer in the shell-side of helically coiled tubes heat exchangers. Enhancement methods for the shell-side can be classified into two types: 'active enhancement' and 'passive enhancement'. Active enhancement typically involves injecting bubbles[24–26] into the shell-side flow to disrupt the flow boundary layer, aiming to enhance heat transfer. Baqir et al. [24]. conducted bubble injection in the shell side of vertically oriented counterflow helically coiled tube heat exchanger, exploring the variations in heat transfer performance under various operating conditions and determining the optimal bubble and shell side flow rates. Their findings indicated that increases in bubble, shell side, and tube side flow rates significantly affected heat transfer efficiency, while having minimal impact on temperature difference. Similar studies include the work of Sadighi et al. [25]., who investigated the influence of bubble injection rates under different flow arrangements on exergy loss and heat transfer efficiency, yielding conclusions consistent with Baqir's. Khorasani and Dadvand[26] injected bubbles into the shell side of horizontally oriented helically coiled tube heat exchanger, demonstrating that bubble motion increased shell side flow turbulence and turbulence intensity, thereby enhancing overall heat transfer efficiency. Passive enhancement is usually achieved by altering the geometric structure to enhance heat transfer. Miansari[27] added circular grooves to the inner wall of the shell-side and conducted comprehensive numerical simulation research. The study demonstrated that the circular groove structure can effectively improve the heat transfer performance of the shell-side with little impact on pressure drop. Andrzejczyk[28] enhanced the heat transfer performance of the shell-side of a single-layer helically coiled tube heat exchanger by using baffles. Experimental results demonstrated that the presence of baffles can effectively improve heat transfer efficiency. Alper[29] proposed a circular baffle that can be used for helically coiled tube heat exchangers. The effectiveness of this baffle was tested and verified through experiments and numerical simulations. The results indicate that the new structure can effectively enhance heat transfer rate and heat transfer coefficient.

From the literature review, it can be observed that most studies on enhanced heat transfer in helically coiled tube heat exchangers focus on the tube-side. This involves altering the shape or surface structure of the helically coiled tube to disturb the flow inside the tube and increase turbulence, thereby improving heat transfer performance. However, there is limited research in enhancing the shell-side heat transfer in

Table 1
Detailed geometric parameters of the heat exchangers.

Geometrical parameters	MHCTHE	DSMHCTHE
Internal diameter of tube 1 and 2 (d_i)	8.12 mm	8.12 mm
External diameter of tube 1 and 2(d_o)	9.52 mm	9.52 mm
Shell diameter (D_S)	140 mm	140 mm
Shell length (L_S)	340 mm	340 mm
Coil diameter of tube 1 (D_1)	50 mm	50 mm
Coil pitch of tube 1 (H_1)	20 mm	20 mm
Coil diameter of tube 2 (D_2)	100 mm	100 mm
Coil pitch of tube 2 (H_2)	20 mm	20 mm
Number of turns of tube 1	15	15
Number of turns of tube 2	15	15
Diameter of inner cylinder (D_{Core1})	—	27 mm
Length of inner cylinder (L_{Core1})	—	320 mm
Diameter of inner cylinder (D_{Core2})	—	77 mm
Length of inner cylinder (L_{Core2})	—	320 mm

helically coiled tube heat exchangers. Additionally, current research on helically coiled tubes heat exchangers mostly adopts a single-layer helically coiled tube structure, while in practical applications, the number of layers in the heat exchanger's helically coiled tubes may be higher. Since enhancing the shell-side heat transfer is one effective method to significantly improve heat exchanger efficiency. Therefore, this study proposes a double shell-passes configuration for a multi-layer helically coiled tubes heat exchanger using passive heat transfer enhancement, referred to as the Double Shell-passes Multi-layer Helically Coiled Tubes Heat Exchanger (DSMHCTHE). In contrast to previous studies, DSMHCTHE introduces a double-layer baffle structure in the shell-side, designed to guide the flow direction and facilitate thorough heat exchange between the fluid and the heat transfer tubes, thereby enhancing heat transfer efficiency. Numerical simulations and experimental studies are conducted in this paper, and a comparison is made with a conventional Multi-Layer Helical Tube Heat Exchanger (MHCTHE). The results confirm the superior performance of DSMHCTHE.

2. Model description and simulation method

2.1. Geometry

The geometric parameters of the studied MHCTHE and DSMHCTHE are illustrated in Fig. 2. The geometric model of MHCTHE is shown in Fig. 2**(a)**. MHCTHE consists of two layers of helically coiled tubes with opposite directions, aiming to better disturb the flow of the shell-side fluid. The arrangement of the shell-side and tube-side fluid flow is shown. This paper proposes the double shell-passes multi-layer helically coiled tubes heat exchanger, and the geometric model is shown in Fig. 2 **(b)**. DSMHCTHE features the addition of two layers of guide cylinders with different diameters and concentric arrangement. They are arranged alternately, and the inlet of the shell-side fluid is connected to the inner guide cylinder. The arrangement of fluid flow is also shown in the figure. The purpose of setting guide cylinders is to guide the flow of the shell-side fluid, allowing it to undergo sufficient heat exchange with the helically coiled tubes, thereby improving the heat transfer efficiency of the heat exchanger. The structural parameters of the helically coiled tubes in DSMHCTHE and MHCTHE are the same. The diameter of the inner guide cylinder in DSMHCTHE is $D_{Core1}=0.5\times D_1$, and the diameter of the outer guide cylinder is $D_{Core2}=0.5\times(D_1+D_2)$. The detailed geometric parameters of the heat exchangers are shown in Table 1.

The same boundary conditions are applied to both heat exchangers:

(1) Tube-side fluid inlet temperature, T_{Ti}=333.15 K. Overall tube-side flow rate, m_T=4 L·min^{-1}, with the same flow rate for different helically coiled tubes.
(2) Inlet temperature of shell-side fluid, T_{Si}=291.65 K. Shell-side flow rate, m_S=3 L·min^{-1}.
(3) The tube walls adopt a no-slip conjugate heat transfer boundary, and the outer wall of the shell is set as an adiabatic boundary.
(4) The outlets are both set as no backflow pressure outlets, with an outlet gauge pressure, P_{out}=0 Pa.

2.2. Governing equation

Under steady-state conditions, the governing equations for incompressible fluid can be written as the following form.

Continuity equation:

$$\frac{\partial}{\partial x_i}(u_i)=0 \tag{1}$$

Momentum equation:

$$\frac{\partial}{\partial x_i}(\rho u_i u_j)=-\frac{\partial p}{\partial x_i}+\frac{\partial}{\partial x_j}\left((\mu+\mu_t)\left(\frac{\partial u_i}{\partial x_j}+\frac{\partial u_j}{\partial x_i}\right)\right) \tag{2}$$

Energy eqiatopm:

$$\frac{\partial}{\partial x_i}(\rho u_i T)=\frac{\partial}{\partial x_i}\left(\left(\frac{\mu}{Pr}+\frac{\mu_t}{Pr_t}\right)\frac{\partial T}{\partial x_i}\right) \tag{3}$$

Where u is the velocity component, T is the temperature, ρ is the density of fluid, μ is the dynamic viscosity, λ is the thermal conductivity, c_p is the specific heat capacity, Pr is the Prandtl number.

Different turbulence models are compared, including the standard k-ε model, realizable k-ε model, Reynolds Stress model (RSM) and SST k-ω model. Considering the computational efficiency and prediction accuracy, the standard k-ε model is used as the turbulence model in this study. The Standard k-ε model, proposed by Launder and Spalding [30], is a semi-empirical model and is the most commonly used turbulence model in engineering fluid simulations. Its main advantages include good robustness, economy, a wide range of applicability, and reasonable accuracy. The transport equations under steady-state conditions are shown as follows:

$$\frac{\partial}{\partial x_i}(\rho k u_i)=\frac{\partial}{\partial x_j}\left[\left(\mu+\frac{\mu_t}{\sigma_k}\right)\frac{\partial k}{\partial x_j}\right]+G_k+G_b-\rho\varepsilon-Y_M+S_k \tag{4}$$

$$\frac{\partial}{\partial x_i}(\rho\varepsilon u_i)=\frac{\partial}{\partial x_j}\left[\left(\mu+\frac{\mu_t}{\sigma_\varepsilon}\right)\frac{\partial \varepsilon}{\partial x_j}\right]+C_{1\varepsilon}\frac{\varepsilon}{k}(G_k+C_{3\varepsilon}G_b)-C_{2\varepsilon}\frac{\varepsilon^2}{k}+S_\varepsilon \tag{5}$$

$$\mu_t=\rho C_\mu\frac{k^2}{\varepsilon} \tag{6}$$

Where G_k represents the turbulent kinetic energy generated by the mean velocity gradient, G_b is the turbulent kinetic energy generated by buoyancy, S_k and S_ε represent the terms of user-defined source. According to the literature [31], $C_{1\varepsilon}$,$C_{2\varepsilon}$,C_μ,σ_k and σ_ε are constants with default values: $C_{1\varepsilon}$=1.44,$C_{2\varepsilon}$=1.92,C_μ=0.09,σ_k=1.0,σ_ε=1.3.

The flow space inside the heat exchangers are divided into the tube-side and shell-side regions. The cold and hot fluids enter the heat exchanger through different nozzles, and heat is transferred and exchanged through the tube-walls. Coupling the convective-diffusive mechanisms in the fluid domain with the heat conduction in the solid domain forms a conjugate heat transfer model. The governing equation for the solid region is:

$$\frac{\partial}{\partial t}(\rho_w h)+\nabla\cdot(\vec{v}\rho_w h)=\nabla\cdot(\lambda_w\nabla T)+S_h \tag{7}$$

Where $h=\int_{T_{ref}}^{T}c_p dT$ is the sensible enthalpy, ρ_w is the density of the heat exchanger tube material, λ_w is the thermal conductivity of the tube wall, $\vec{v}$ is related to the motion of the solid region, and S_h is the volumetric heat source term.

This study conducts numerical simulation research on the flow and

Table 2
Grid-independence for the MHCTHE and DSMHCTHE.

		Mesh 1	Mesh 2	Mesh 3	Mesh 4	Mesh 5
MHCTHE	Grids number	116.4 × 10^4	183.5 × 10^4	306.2 × 10^4	481.3 × 10^4	597.4 × 10^4
	T_{So}	307.79	308.96	309.76	309.82	309.86
	$\overline{T}_{To}$	321.04	320.17	319.57	319.52	319.49
DSMHCTHE	Grids number	178.9 × 10^4	265.7 × 10^4	368.4 × 10^4	553.8 × 10^4	672.5 × 10^4
	T_{So}	310.28	311.72	312.37	312.44	312.39
	$\overline{T}_{To}$	319.18	318.10	317.61	317.56	317.60

heat transfer performance of the helically coiled tubes heat exchangers under steady-state, non-phase-change conditions. Since there is no rotation or translation motion of the solid, Eq. (7) can be written as:

$$\nabla\cdot(\lambda_w \nabla T) = 0 \tag{8}$$

2.3. Meshing

The number of grids can affect the results of numerical simulations, grids independence verification is necessary. Five sets of grids were generated for MHCTHE and DSMHCTHE, and the corresponding temperature changes at the outlet are shown in Fig. 4. The grids numbers and temperatures are listed in Table 2. The wall functions affect the solution of the flow law in the boundary layer. With the increasing of grids, the $y+$ varies in the range of 25 to 1 at tube-side. Therefore, the enhanced wall treatment method was adopted in this study. It can be observed that from the third set of grids onward, the calculated outlet temperature hardly changes with an increase in the number of grids. The meshing method of the third set of grids was adopted, and the corresponding grid settings are as follows: the first layer near the wall has a grid size of 0.1 mm with a total of 7 inflation layers. The near-wall grid growth rate is 1.2, the face grid size ranges from a minimum of 1 mm to a maximum of 9 mm, and the volume grid uses the Polyhexdra form. Fig. 3 presents the generated mesh of the heat exchangers. The commercial software FLUENT was employed for numerical simulation. The finite volume method was adopted for discrete governing equations, and the discrete format was a second-order upwind scheme. The SIMPLE algorithm was implemented to solve the coupling of pressure and velocity. The convergence was set to a residual of less than 10^{-5} for the continuity and momentum equations and less than 10^{-6} for the energy equations.

3. Experiment setup and data processing

3.1. Experiment setup

The experimental system comprises the tested heat exchanger, a thermostatic water storage tank, a circulation pump, an electric heating device, measurement systems, valves, and pipelines. As shown in Fig. 5, the experimental system consists of two circuits: the hot fluid circuit passing through the helically coiled tubes and the cold fluid circuit passing through the shell-side of the heat exchanger. At the inlet of the heat exchanger, the hot fluid is divided into two branches, each

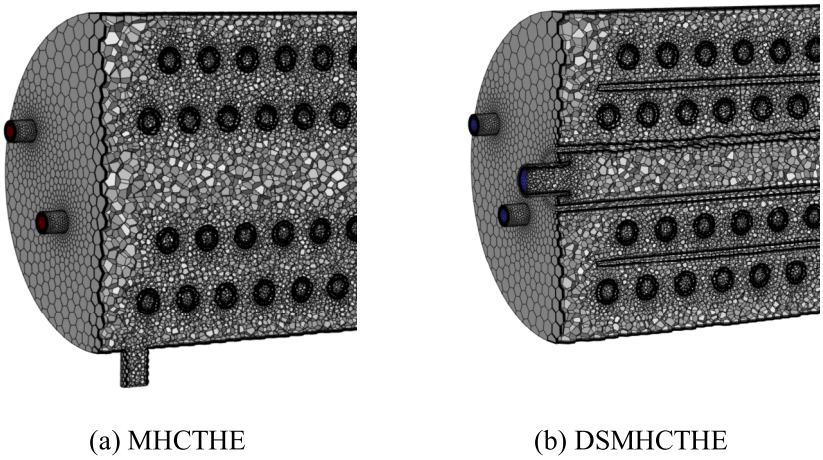

Fig. 3. Generated mesh for the heat exchangers.

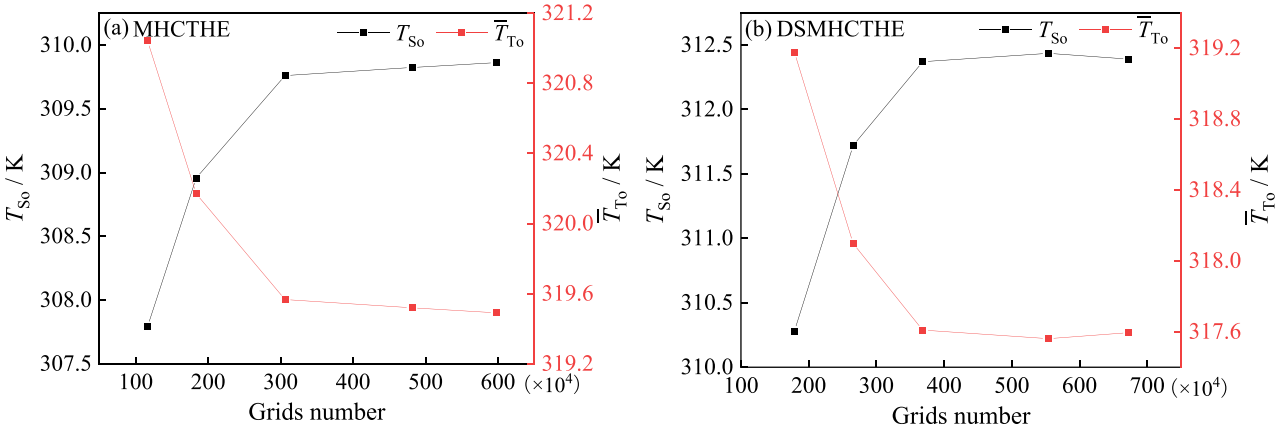

Fig. 4. Grids independence verification of the MHCTHE and DSMHCTHE.

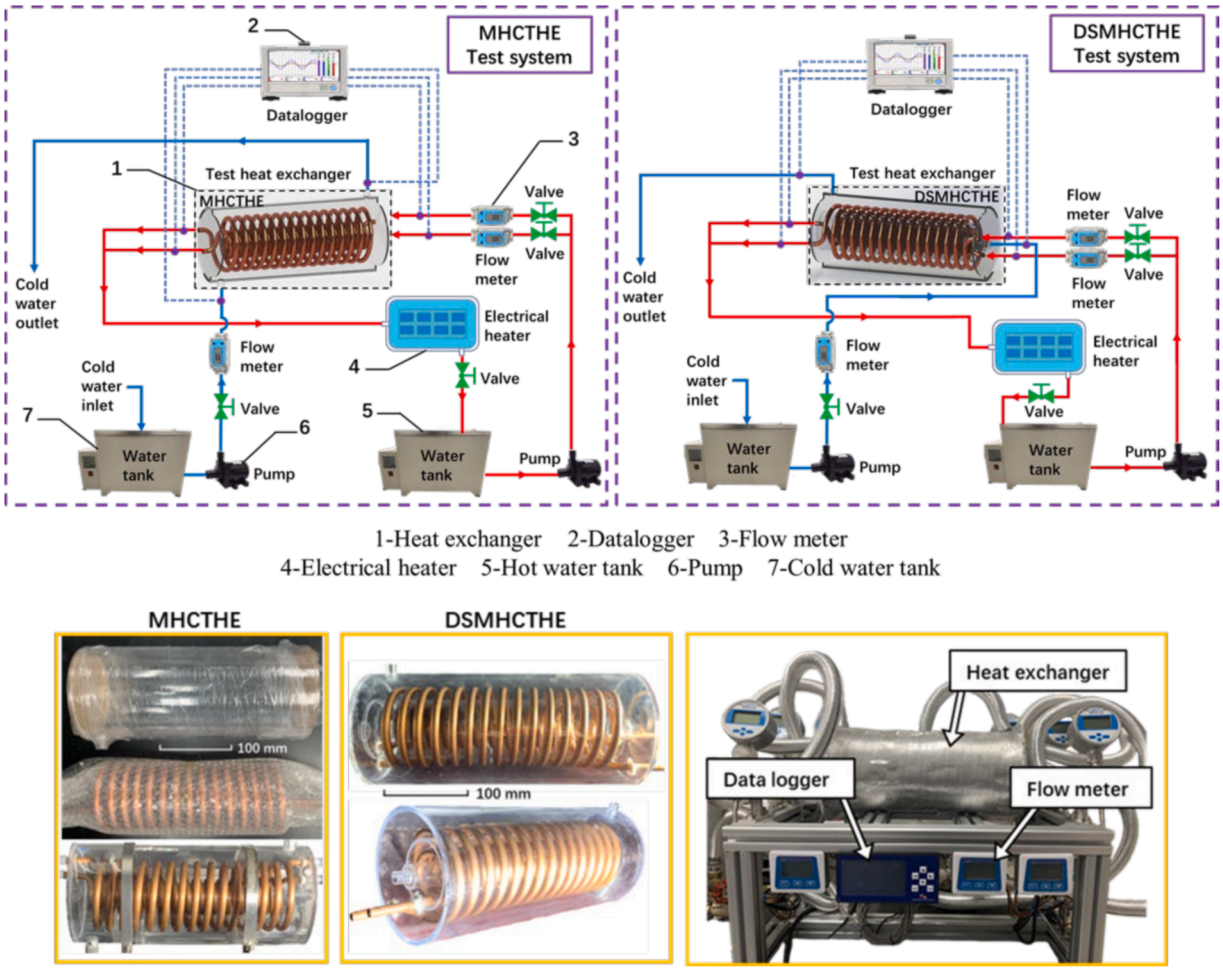

Fig. 5. Experimental system diagram.

Table 3
Experimental condition parameter range.

	Total flow rate in tube-side (m_T)	Total flow rate in shell-side (m_S)	Inlet temperature of tube-side flow (T_{Ti})	Inlet temperature of shell-side flow (T_{Si})
Operating condition	2–6 L·min^{-1}	2–5 L·min^{-1}	50–70 °C	18.5 °C

controlled by an individual valve and equipped with a flowmeter. After heat exchange in the tested heat exchanger, the hot fluid with reduced temperature flows through the electric heating device, reaches the set temperature, and returns to the thermostatic water storage tank. The cold fluid exits the heat exchanger and is discharged. Moreover, the physical appearance of MHCTHE and DSMHCTHE are displayed, along with a snapshot of the experimental setup.

The heat exchanger is composed of helically coiled copper tubes and an acrylic shell, with seams at the connections sealed using waterproof materials. Before integrating the heat exchanger into the experimental system, a water tightness test is conducted at atmospheric pressure to ensure complete sealing. Additionally, the heat exchanger and pipelines are wrapped with insulation material and aluminum foil to reduce heat dissipation between the experimental system and the environment.

The data to be measured in the experimental system includes the following: all outlet temperatures of the tested heat exchanger, flow rates in all circuits (including branches), and the pressure differentials between the corresponding inlet and outlet of the heat exchanger. Additionally, it is necessary to monitor the temperatures at each inlet of the heat exchanger.

The variables for the experimental conditions are as follows: shell-side volumetric flow rate (m_S), tube-side volumetric flow rate (m_T), and the maximum temperature difference across the heat exchanger (ΔT_{max}, i.e., the difference between the cold and hot inlet temperatures). The operational parameters are listed in Table 3, with the shell-side flow rate ranging from 2 to 5 L·min^{-1}, and the tube-side branch (per layer of tubes) flow rate varying from 1 to 3 L·min^{-1}. The shell-side represents the cold fluid with an inlet temperature of 18.5 °C, while the tube-side represents the hot fluid with an inlet temperature ranging from 50 to 70 °C. The Hall pulse flow sensor is used to collect the flow. The flow ranges of shell and tube branches are 1~20 L·min^{-1} and 0.3~3 L·min^{-1}, respectively, with an accuracy of 3 %FS. The accuracy of the thermocouple after calibration test is about ±0.2 °C. The Pressure sensor has a measuring range of 0~50 kPaG and an accuracy of ±0.1 %FS.

3.2. Data processing

The heat transfer rates Q_S and Q_T for the shell-side and tube-side fluids, respectively, are given by:

$$Q_S = m_S \rho_S c_{p,s} |T_{So} - T_{Si}| \tag{9}$$

$$Q_T = m_T \rho_T c_{p,t} |\overline{T}_{To} - T_{Ti}| \tag{10}$$

The total heat transfer rate of the heat exchangers is represented by the average heat transfer rate Q of the cold and hot fluids:

$$Q = \frac{m_T \rho_T c_{p,t} \left| \overline{T}_{To} - T_{Ti} \right| + m_S \rho_S c_{p,s} \left| T_{So} - T_{Si} \right|}{2} \tag{11}$$

Where m_T and m_S are the volumetric flow rates of the tube-side and shell-side, respectively. ρ_T and ρ_S are the densities of the tube-side and shell-side fluids, $c_{p,t}$ and $c_{p,s}$ are the specific heat capacities at constant pressure for the tube-side and shell-side fluids. T_{Ti} and T_{To} are the inlet and outlet temperatures of the tube-side fluid, while T_{Si} and T_{So} are the inlet and outlet temperatures of the shell-side fluid.

The total heat transfer rate also satisfies the following equation:

$$Q = \varphi U_o A_o \Delta T_{LMTD} \tag{12}$$

$$\Delta T_{LMTD} = \frac{(T_{Si} - \overline{T}_{To}) - (T_{So} - T_{Ti})}{\ln[(T_{Si} - \overline{T}_{To})/(T_{So} - T_{Ti})]} \tag{13}$$

Where φ is the temperature difference correction factor, which is obtained by table lookup and is less than 1. ΔT_{LMTD} is the logarithmic mean temperature difference of the heat exchanger, A_o is the heat transfer area calculated based on the tube outer diameter, and U_o is the overall heat transfer coefficient of the heat exchanger.

$$\frac{1}{U_o} = \frac{1}{h_S} + \frac{d_o}{d_i}\frac{1}{h_T} + \frac{d_o}{2\lambda_w}\ln\left(\frac{d_o}{d_i}\right) \tag{14}$$

Where h_T and h_S are the heat transfer coefficients for the tube-side and shell-side, respectively.

The calculation method for the Nusselt number is:

$$Nu = \frac{hD_h}{\lambda} \tag{15}$$

Where λ is the thermal conductivity of the fluid. D_h is the hydraulic diameter. For the tube-side, D_h=d_i, while for the shell-side, the calculation of D_h is as follows:

$$D_h = \frac{4V_S}{A_S} \tag{16}$$

Where V_S is the volume of shell-side domain, A_S is the contact area of fluid on shell-side.

The calculation method for the Reynolds number is:

$$Re = \frac{4m\rho}{\mu\pi D_h} \tag{17}$$

The calculation method for the heat transfer coefficient on the tube-side is as follows[6]:

$$Re_{cr} = 20,000(d/D)^{0.32} \tag{18}$$

If Re<Re_{cr}, Manlapaz's correlation [32] is used:

$$Nu = \left[\left(3.657 + \frac{4.343}{(1 + 957/(PrHe^2))^2}\right)^3 + 1.158\left(\frac{He}{1 + 0.477/Pr}\right)^{3/2}\right]^{1/3} \tag{19}$$

If Re>Re_{cr}, Rogers' correlation [33] is used:

$$Nu = 0.023Re^{0.85}Pr^{0.4}(d/D)^{0.1} \tag{20}$$

The shell-side heat transfer coefficient is calculated according to the following equation:

$$h_S = \left[\frac{1}{U_o} - \frac{d_o}{d_i}\frac{1}{h_T} - \frac{d_o}{2\lambda_w}\ln\left(\frac{d_o}{d_i}\right)\right]^{-1} \tag{21}$$

The thermal effectiveness (ε) represents the ratio of the actual heat transfer rate under given conditions to the theoretical maximum heat transfer rate. It is commonly used to assess the heat transfer capability of a heat exchanger and ranges between 0 and 1. A higher value indicates a stronger heat transfer capability. The calculation method is as follows:

$$\varepsilon = \frac{Q}{Q_{max}} = \frac{Q}{(Mc_p)_{min}|T_{Si} - T_{Ti}|} \tag{22}$$

However, evaluating the heat exchanger solely based on thermal effectiveness is evidently not objective, as an increase in thermal effectiveness might lead to an increase in pressure loss for the heat exchanger. To explore the potential of DSMHCTHE, a comprehensive evaluation criterion considering both heat transfer and pressure drop is necessary. The comprehensive performance (ξ) of the heat exchanger, an important indicator for assessing its performance, is calculated as follows:

$$\xi = \frac{Q}{W_P} = \frac{Q}{\sum m\Delta P} \tag{23}$$

From equation (23), it can be observed that the comprehensive performance is defined as the ratio of the average heat transfer rate and pump power (W_P). A higher ξ indicates better heat transfer performance under the same pump power, making it suitable for comparing the performance of different heat exchangers.

3.3. Uncertainty acquisition

The method for calculating the uncertainty of the target variables is as follows:

$$|\delta U_w| = \sqrt{\left(\frac{\partial w}{\partial x_1}\delta x_1\right)^2 + \left(\frac{\partial w}{\partial x_2}\delta x_2\right)^2 + \cdots + \left(\frac{\partial w}{\partial x_n}\delta x_n\right)^2} \tag{24}$$

In the equation, w represents the target variable, where x_1 to x_n are indirectly contributing independent variables, and there exists a mapping relationship $w = f(x_1,x_2,\ldots,x_n)$. The relative uncertainty of w, denoted as U_w, is calculated as follows:

$$U_w = \left|\frac{\delta U_w}{w}\right| \times 100\% \tag{25}$$

The uncertainty of the heat transfer rate (Q) is given by:

$$\begin{aligned}\delta Q_S &= \sqrt{\left(\frac{\partial Q_S}{\partial M_S}\delta M_S\right)^2 + \left(\frac{\partial Q_S}{\partial T_{Si}}\delta T_{Si}\right)^2 + \left(\frac{\partial Q_S}{\partial T_{So}}\delta T_{So}\right)^2} \\ &= \rho_S m_S c_{p,s}\sqrt{[(T_{So} - T_{Si})\delta m_S]^2 + (\delta T_{Si})^2 + (\delta T_{So})^2}\end{aligned} \tag{26}$$

$$\begin{aligned}\delta Q_T &= \sqrt{2\left[\left(\frac{\partial Q_T}{\partial M_T}\delta M_T\right)^2 + \left(\frac{\partial Q_T}{\partial T_{Ti}}\delta T_{Ti}\right)^2 + \left(\frac{\partial Q_T}{\partial T_{To}}\delta T_{To}\right)^2\right]} \\ &= \sqrt{2}\rho_T m_T c_{p,t}\sqrt{[(T_{To} - T_{Ti})\delta m_T]^2 + (\delta T_{Ti})^2 + (\delta T_{To})^2}\end{aligned} \tag{27}$$

$$\delta Q = \delta Q_S + \delta Q_T \tag{28}$$

The uncertainty of the logarithmic mean temperature difference (ΔT_{LMTD}) is expressed as:

$$\delta(\Delta T_{LMTD}) = \sqrt{\begin{aligned}&\left[\frac{1}{\ln\frac{\Delta T_1}{\Delta T_2}} - \frac{(\Delta T_1 - \Delta T_2)}{\Delta T_1\left(\ln\frac{\Delta T_1}{\Delta T_2}\right)^2}\right]^2 \delta(\Delta T)^2 \\ &+ \left[\frac{-1}{\ln\frac{\Delta T_1}{\Delta T_2}} + \frac{(\Delta T_1 - \Delta T_2)}{\Delta T_2\left(\ln\frac{\Delta T_1}{\Delta T_2}\right)^2}\right]^2 \delta(\Delta T)^2\end{aligned}} \tag{29}$$

The overall heat transfer coefficient (U_o), determined by equation (14), is evaluated for uncertainty using the following method:

Table 4
Main uncertainties of the experimental systems.

	MHCTHE	DSMHCTHE
Heat transfer rate (Q)	±1.78 %	±1.82 %
logarithmic mean temperature difference (ΔT_{LMTD})	±1.21 %	±1.39 %
Overall heat transfer coefficient (U_o)	±3.71 %	±3.82 %
Shell-side heat transfer coefficient (h_{S})	±5.47 %	±5.71 %
Thermal effectiveness (ε)	±5.79 %	±5.75 %
Comprehensive performance (ξ)	±3.05 %	±2.84 %
Pressure drop (ΔP)	±0.2 %	±0.2 %

$$\delta U_o = \sqrt{\left[\frac{\delta(Q)}{A_o \Delta T_{\mathrm{LMTD}}}\right]^2 + \left[\frac{Q\delta(\Delta T_{\mathrm{LMTD}})}{A_o(\Delta T_{\mathrm{LMTD}})^2}\right]^2} \tag{30}$$

The uncertainty of the shell-side heat transfer coefficient (h_{S}) is calculated as follows:

$$\delta h_{\mathrm{S}} = \sqrt{\left[\frac{\partial\left(U_o^{-1}+c\right)}{\partial U_o}\delta U_o\right]^2} = \frac{1}{(cU_o+1)^2}\delta U_o \tag{31}$$

where $c = -\left[\frac{d_o}{d_i h_{\mathrm{T}}} + \frac{d_o}{2\lambda_w}\ln\left(\frac{d_o}{d_i}\right)\right]$.

The uncertainty of the thermal effectiveness (ε) is expressed as:

$$\delta\varepsilon = \sqrt{\begin{array}{c}\left[\frac{\delta Q_{\mathrm{ave}}}{Mc_p(T_{\mathrm{Si}}-T_{\mathrm{Ti}})}\right]^2 + \left[\frac{Q_{\mathrm{ave}}}{c_p(T_{\mathrm{Si}}-T_{\mathrm{Ti}})}\frac{\delta M}{M^2}\right]^2 \\ + \left(\frac{Q_{\mathrm{ave}}}{Mc_p}\frac{\delta T}{T_{\mathrm{Si}}}\right)^2 + \left(\frac{Q_{\mathrm{ave}}}{Mc_p}\frac{\delta T}{T_{\mathrm{Ti}}}\right)^2\end{array}} \tag{32}$$

The uncertainty of the pump power (W_{P}) is expressed as:

$$\delta(W_{\mathrm{P}}) = \sqrt{[\Delta P_{\mathrm{S}}\delta(m_{\mathrm{S}})]^2 + [\Delta P_{\mathrm{T}}\delta(m_{\mathrm{T}})]^2 + [m_{\mathrm{S}}\delta(\Delta P_{\mathrm{S}})]^2 + [m_{\mathrm{T}}\delta(\Delta P_{\mathrm{T}})]^2} \tag{33}$$

The uncertainty of the comprehensive performance (ξ) is expressed as:

$$\delta(\xi) = \sqrt{\left[\frac{\delta(Q)}{W_{\mathrm{P}}}\right]^2 + \left[\frac{Q}{W_{\mathrm{P}}^2}\delta(W_{\mathrm{P}})\right]^2} \tag{34}$$

The uncertainties for the measured parameters are calculated and

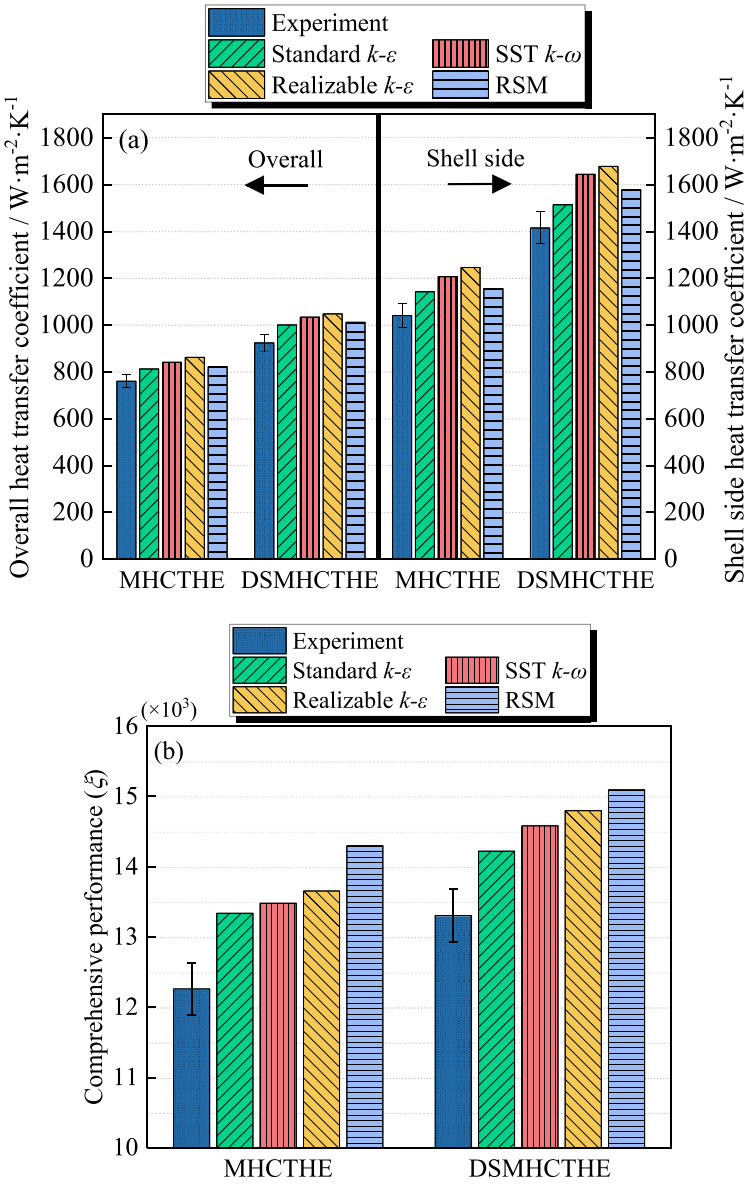

Fig. 6. Verification of experimental results of helically coiled tubes heat exchangers.

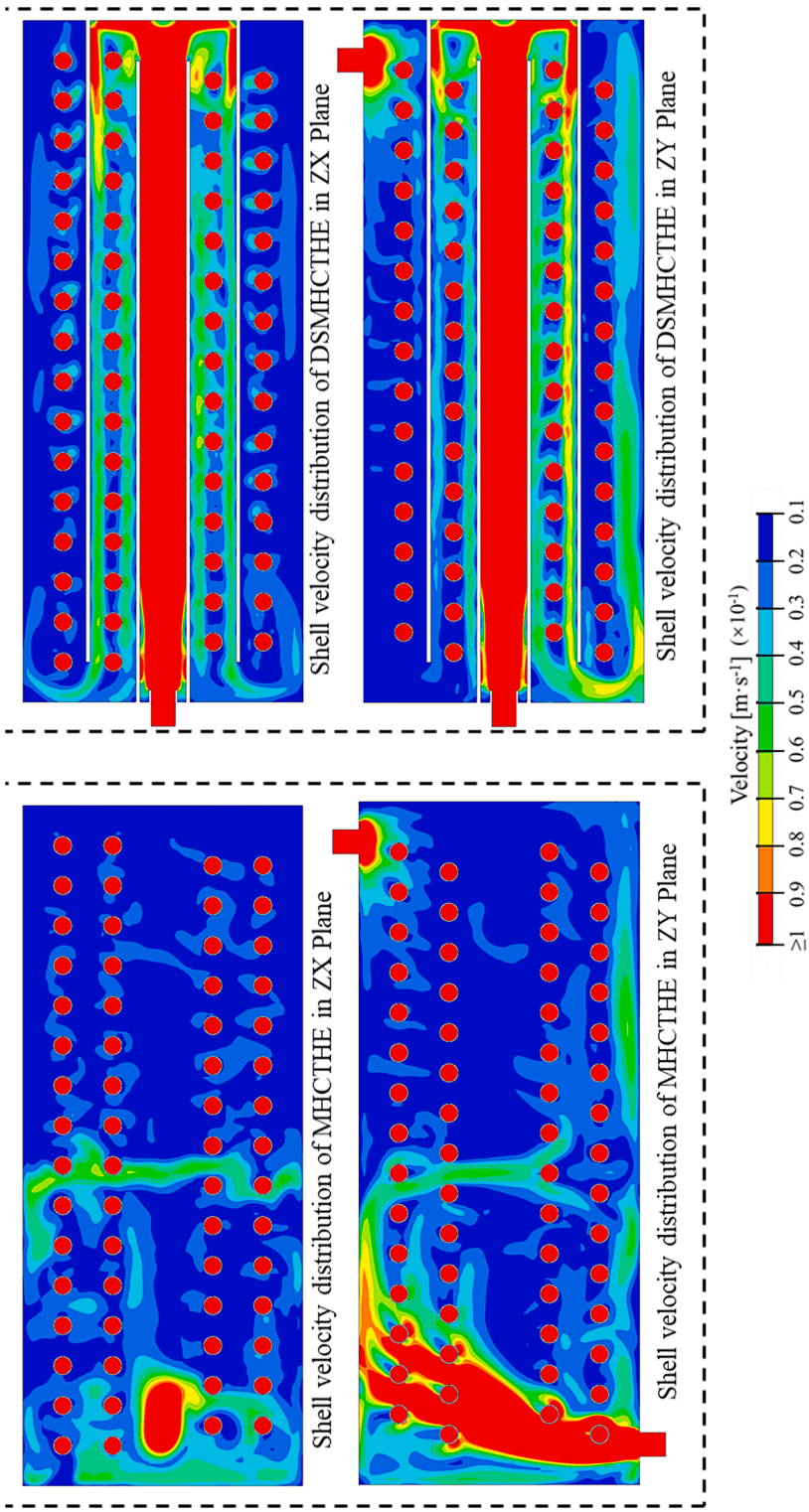

Fig. 7. Velocity contour of MHCTHE and DSMHCTHE in cross sections.

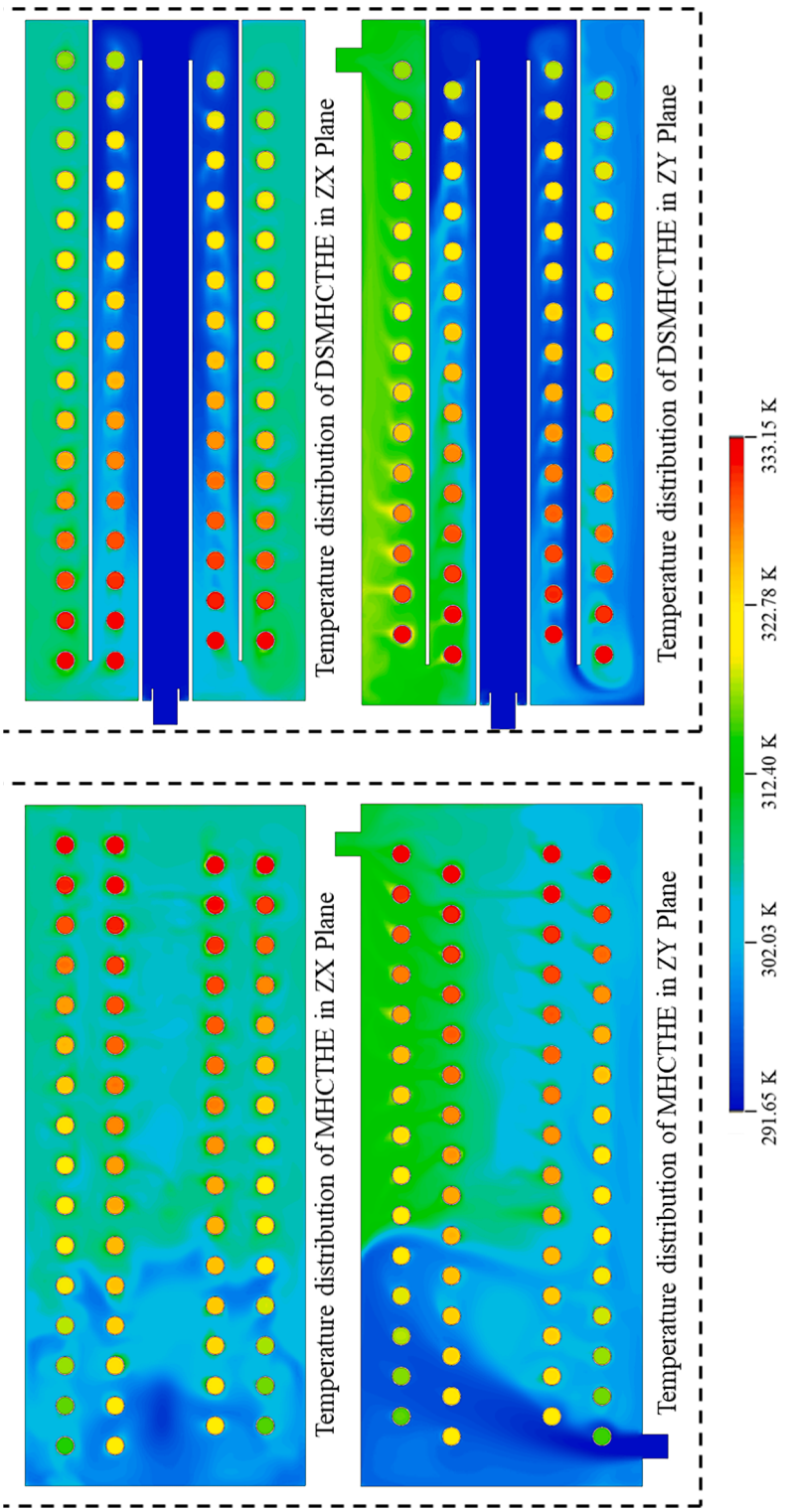

Fig. 8. Temperature contour of MHCTHE and DSMHCTHE in cross sections.

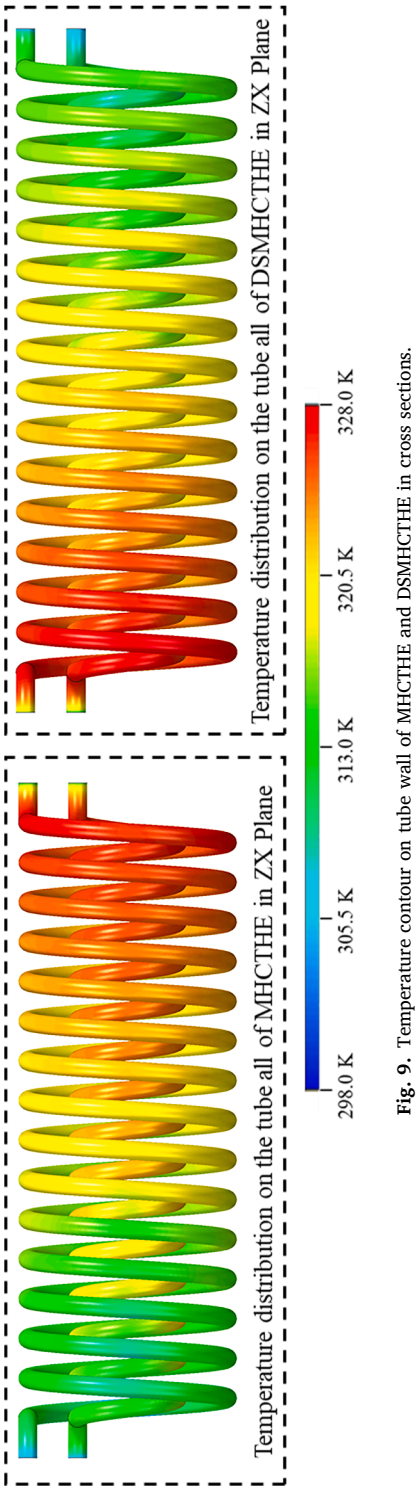

Fig. 9. Temperature contour on tube wall of MHCTHE and DSMHCTHE in cross sections.

listed in Table 4. It can be observed that the uncertainties in the experimental measurements in this study are within a reasonably acceptable range, indicating a high level of accuracy in the obtained data.

4. Numerical model validation

The simulation results of the heat transfer coefficients and the comprehensive performance are verified by the experimental data, as illustrated in Fig. 6. From the comparative results in Fig. 6**(a)**, it presents the comparison between the experimentally obtained total heat transfer coefficient, shell-side heat transfer coefficient, and different turbulence models. The maximum deviation in total heat transfer coefficient is 6.49 % to 13.5 %, and for the shell-side heat transfer coefficient, it is 8.90 % to 19.7 %. Fig. 6**(b)** presents the deviation of the comprehensive performance of the heat exchanger obtained by numerical simulation is 8.48 % to 16.6 % compared with the experimental data. For the heat transfer coefficient, the performance of standard k-ε model and Reynolds Stress model are closer to the experimental value, while for the comprehensive performance of the heat exchanger, standard k-ε model is closer to the experimental value. Therefore, it is more appropriate to choose standard k-ε model as turbulence model.

5. Results and discussion

5.1. Simulation results

Fig. 7 illustrates the velocity distribution contours for MHCTHE and DSMHCTHE, while Figs. 8-9 present temperature contours for both heat exchangers (m_S=3 L·min^{-1}, m_T=4 L·min^{-1}). The design of the double shell-passes structure improves the uneven shell-side velocity distribution and low velocity issues, moreover, the temperature of DSMHCTHE at shell-side outlet is higher than that of MHCTHE. This means that the shell fluid of DSMHCTHE obtains more heat from the tubes, and the heat transfer efficiency of the heat exchanger is improved. The total heat transfer rate of DSMHCTHE is 4499 W, which represents a 7.3 % improvement compared to MHCTHE. Calculations reveal that the total heat transfer coefficient and shell-side heat transfer coefficient for MHCTHE are 812 W·m^{-2}·K^{-1} and 1143 W·m^{-2}·K^{-1}, respectively. Under the same operating conditions, DSMHCTHE achieves total heat transfer and shell-side heat transfer coefficients of 1000 W·m^{-2}·K^{-1} and 1554 W·m^{-2}·K^{-1}, respectively, marking a 23.2 % and 36.0 % enhancement compared to MHCTHE.

5.2. Experimental results

Figs. 10-11 depict the variations in heat transfer rate for MHCTHE and DSMHCTHE with changes in flow rate and fluid inlet temperature difference. From the figures, it is evident that both types of heat exchangers exhibit similar trends, wherein the heat transfer rate increases with an increase in flow rate on either side. With an increase in shell-side flow rate, the heat transfer rate for MHCTHE increases by 14.2 % to 46.3 %, while for DSMHCTHE, it increases by 13.8 % to 47.1 %. As the tube-side flow rate increases, the heat transfer rate for MHCTHE increases by 15.7 % to 56.7 %, and for DSMHCTHE, it increases by 17.9 % to 61.3 %. Additionally, the heat transfer rate increases with an increase in the inlet temperature difference between the cold and hot fluids. When the inlet temperature increases from 50 °C to 70 °C, the heat transfer rate for MHCTHE and DSMHCTHE increases by 77.1 % and 75.3 %, respectively. Under the same experimental conditions, DSMHCTHE exhibits a 5.1 % to 12.9 % higher heat transfer rate compared to MHCTHE. It can be observed that an increase in flow rate on either side leads to a rise in the total heat transfer rate. Moreover, an increase in the temperature difference at the fluid inlet further enhances the heat transfer. This pattern applies to the two kinds of heat exchangers. Additionally, the structure of DSMHCTHE can further reinforce the effectiveness of heat transfer.

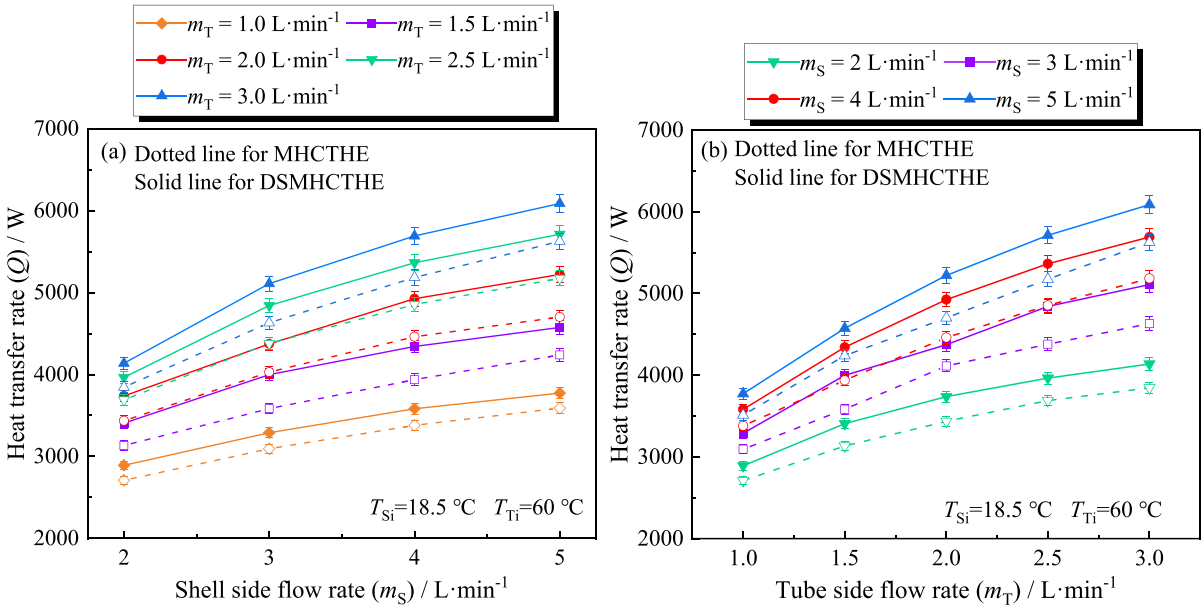

Fig. 10. Variation of heat transfer rate with flow rate of the heat exchangers.

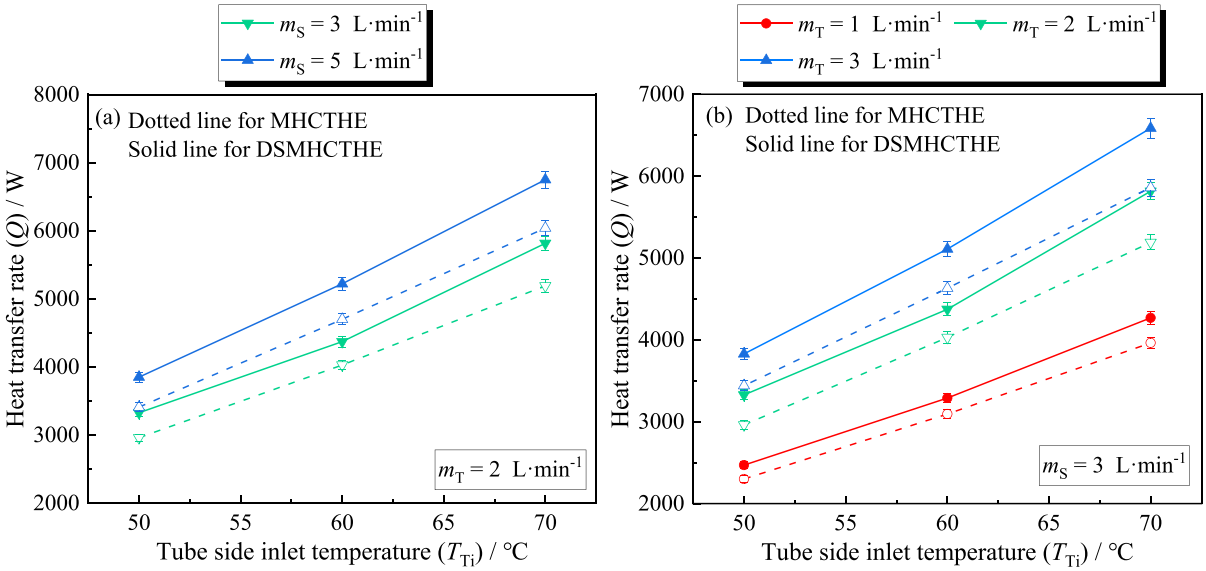

Fig. 11. Variation of heat transfer rate with inlet temperature difference of the heat exchangers.

This enhancement stems from the presence of flow deflection structures, which redistribute fluid flow, augmenting flow velocities near the helical tubes and thereby reinforcing heat transfer effects, particularly evident at higher flow rates.

Figs. 12-13 illustrate the variations in the total heat transfer coefficient for MHCTHE and DSMHCTHE with changes in flow rate and fluid inlet temperature difference. From the figures, it is observed that with an increase in flow rate or an increase in inlet temperature difference, the total heat transfer coefficient for both types of heat exchangers shows an increasing trend. As the shell-side flow rate increases, the total heat transfer coefficient for MHCTHE increases by 10.8 % to 24.5 %, while for DSMHCTHE, it increases by 5.5 % to 26.3 %. With an increase in tube-side flow rate, the total heat transfer coefficient for MHCTHE increases by 7.7 % to 38.5 %, and for DSMHCTHE, it increases by 11.0 % to 41.4 %. When the inlet temperature increases from 50 °C to 70 °C, the total heat transfer coefficient for MHCTHE and DSMHCTHE increases by 12.8 % and 11.7 %, respectively. Under the same operating conditions, DSMHCTHE exhibits a 21.5 % to 29.0 % higher total heat transfer coefficient compared to MHCTHE. For both types of heat exchangers, the trends induced by operational variations are similar, while the new flow pattern is one of the primary reasons for DSMHCTHE having a higher heat transfer coefficient.

Figs. 14-15 present the variations in the shell-side heat transfer coefficient for MHCTHE and DSMHCTHE with changes in flow rate and fluid inlet temperature difference. The shell-side heat transfer coefficient shows an increasing trend with an increase in flow rate and is also influenced by an increase in inlet temperature difference. Under the same operating conditions, DSMHCTHE exhibits a shell-side heat transfer coefficient 36.2 % to 47.5 % higher than that of MHCTHE.

Figs. 16-17 depict the variations in heat transfer effectiveness for MHCTHE and DSMHCTHE with changes in flow rate and fluid inlet temperature difference. It can be observed that the trends in thermal effectiveness for both types of heat exchangers are generally similar. In this experiment, the shell-side fluid is the cold fluid, and the tube-side

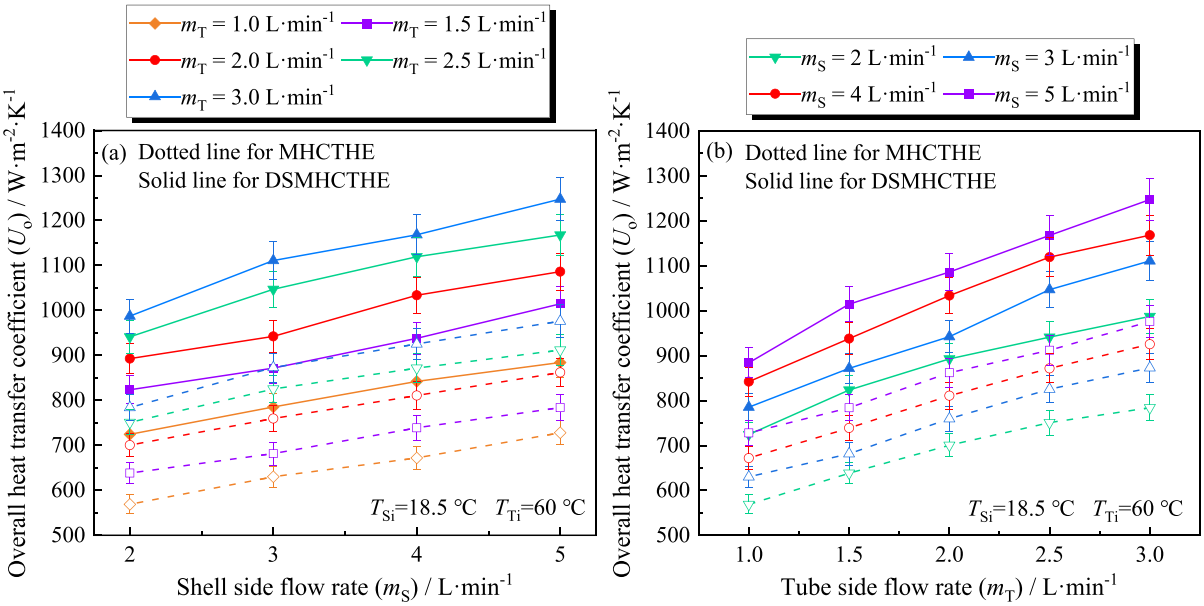

Fig. 12. Variation of overall heat transfer coefficient with flow rate of the heat exchangers.

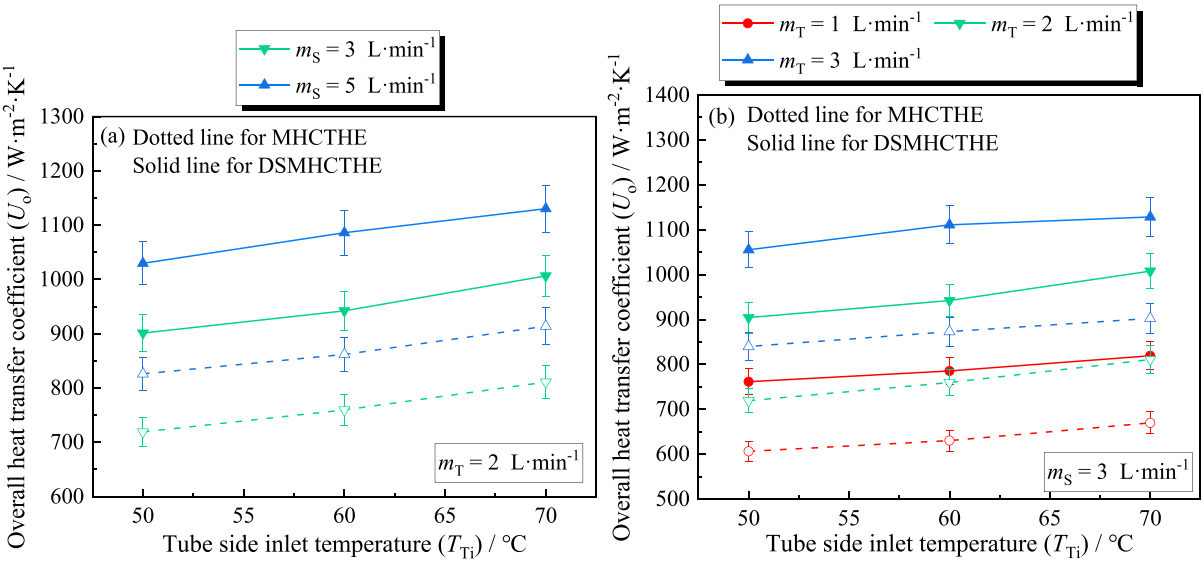

Fig. 13. Variation of overall heat transfer coefficient with inlet temperature difference of the heat exchangers.

fluid is the hot fluid. The thermal effectiveness of the heat exchanger decreases with an increase in shell-side flow rate and increases with an increase in tube-side flow rate. This is because in the calculation of thermal effectiveness in this study, the theoretical maximum heat transfer rate is calculated based on the heat capacity of the cold fluid. While increasing the shell-side flow rate enhances heat transfer, the actual rate of increase in heat transfer is lower than the theoretical maximum heat transfer rate.

With an increase in shell-side flow rate, the thermal effectiveness of MHCTHE decreases by 18.2 % to 47.8 %, and that of DSMHCTHE decreases by 17.7 % to 47.8 %. As the tube-side flow rate increases, the thermal effectiveness of MHCTHE increases by 14.0 % to 56.1 %, and that of DSMHCTHE increases by 17.9 % to 61.3 %. With a constant flow rate, there is no significant change in the thermal effectiveness of both heat exchangers when the inlet temperature increases from 50 °C to 70 °C. Under the same operating conditions, DSMHCTHE exhibits a thermal effectiveness 5.1 % to 12.9 % higher than that of MHCTHE.

Table 5 presents a comparison between the research results of this study and similar studies on helically coiled tube heat exchangers, including the flow rates, total heat transfer, and heat transfer coefficients adopted under experimental conditions. The overall heat transfer coefficients for MHCTHE ranged from 569 to 976 W·m^{-2}·K^{-1}, while for DSMHCTHE, the overall heat transfer coefficients ranged from 724 to 1247 W·m^{-2}·K^{-1} under the experimental conditions. It is evident that DSMHCTHE performs better than MHCTHE. Jamshidi et al. [9]. conducted experimental research on helically coiled tube heat exchangers and obtained total heat transfer coefficients ranging from 475 to 1143 W·m^{-2}·K^{-1}. Ghorbani et al. [12]. experimentally tested helically coiled tube heat exchanger, with total heat transfer coefficients ranging from 405 to 1200 W·m^{-2}·K^{-1}. Alper et al. [29]. numerically simulated and experimentally investigated helically coiled tube heat exchanger with circular baffle plates, with total heat transfer coefficients ranging from 800 to 1400 W·m^{-2}·K^{-1}. Panahi et al. [34]. conducted experimental research by placing disturbance wires inside the helically coiled tube as elements for enhancing heat transfer, with total heat transfer coefficients ranging from 475 to 1700 W·m^{-2}·K^{-1}. Comparing

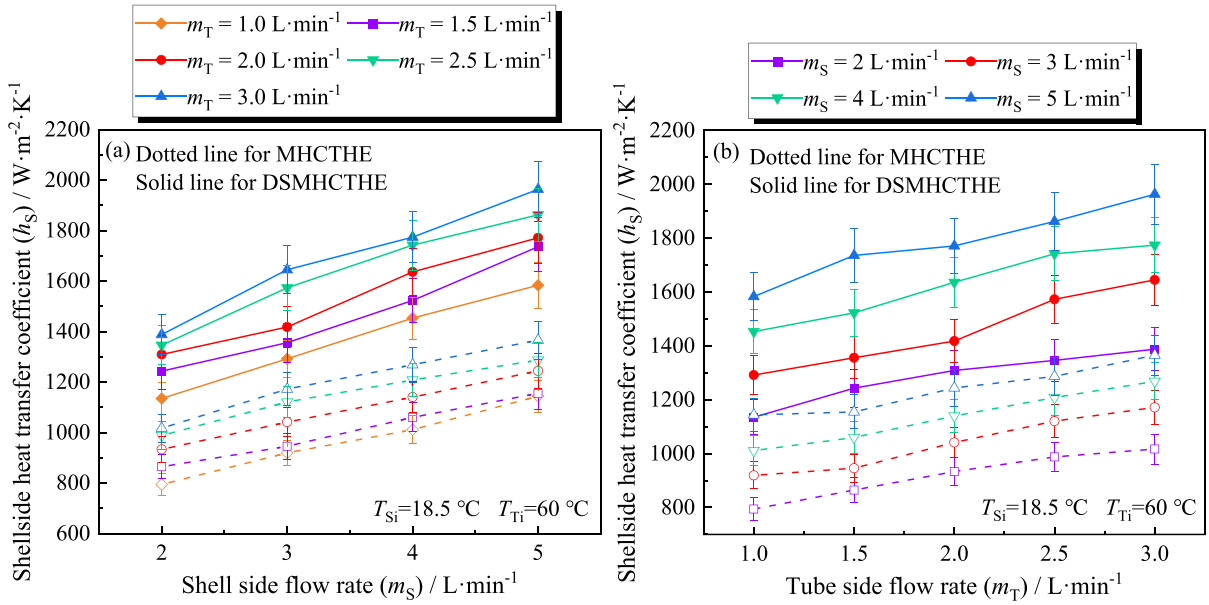

Fig. 14. Variation of shell-side heat transfer coefficient with flow rate of the heat exchangers.

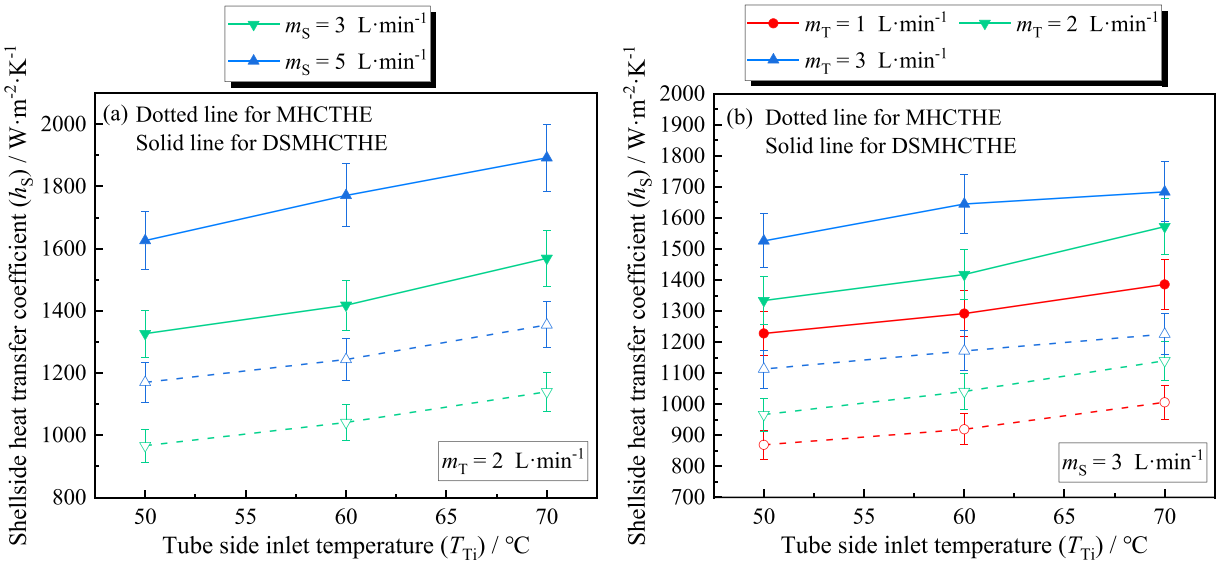

Fig. 15. Variation of shell-side heat transfer coefficient with inlet temperature difference of the heat exchangers.

the research results of this study with similar literature reveals consistency in performance variations. It is noteworthy that due to differences in structural parameters or experimental conditions among various studies, direct measurement and comparison of different works are challenging. Nevertheless, the results of this study are in good agreement with similar literature.

Fig. 18 illustrates the variations in pressure drop on both sides of the heat exchanger with changes in flow rate. With an increase in shell-side flow rate, the shell-side pressure drop for DSMHCTHE is 60.7 % to 83.4 % higher than that of MHCTHE. However, the tube-side pressure drop for both heat exchangers shows a minor difference, with the outer layer of helically coiled tubes having a pressure drop 61.6 % to 68.3 % higher than the inner layer.

Fig. 19 presents a comparison of the comprehensive performance of the heat exchanger under different flow rates and inlet temperature differences. The ratio of the comprehensive performance of DSMHCTHE to MHCTHE is used as the vertical axis. A ratio greater than 1 indicates that DSMHCTHE can provide a stronger heat transfer effect while consuming the same pump power. As shown in Fig. 19**(a)**, the ratio increases first and then decreases with an increase in shell-side flow rate. In Fig. 19**(b)**, the ratio increases initially and then levels off with an increase in tube-side flow rate, with the increment diminishing as the tube-side flow rate increases. This is because, under the experimental conditions, the tube-side pressure drop is significantly higher than the shell-side pressure drop. Increasing the flow rate on either side can enhance the total heat transfer rate to some extent, and the tube-side pressure drop difference between the two heat exchangers is minimal. DSMHCTHE can obtain more heat transfer, and under the experimental conditions, the ratio of its comprehensive performance can reach 1.12. In Fig. 19**(c)**, the ratio of comprehensive performance remains relatively constant with an increase in inlet temperature difference, indicating that the ratio of comprehensive performance is not significantly affected by the inlet temperature difference.

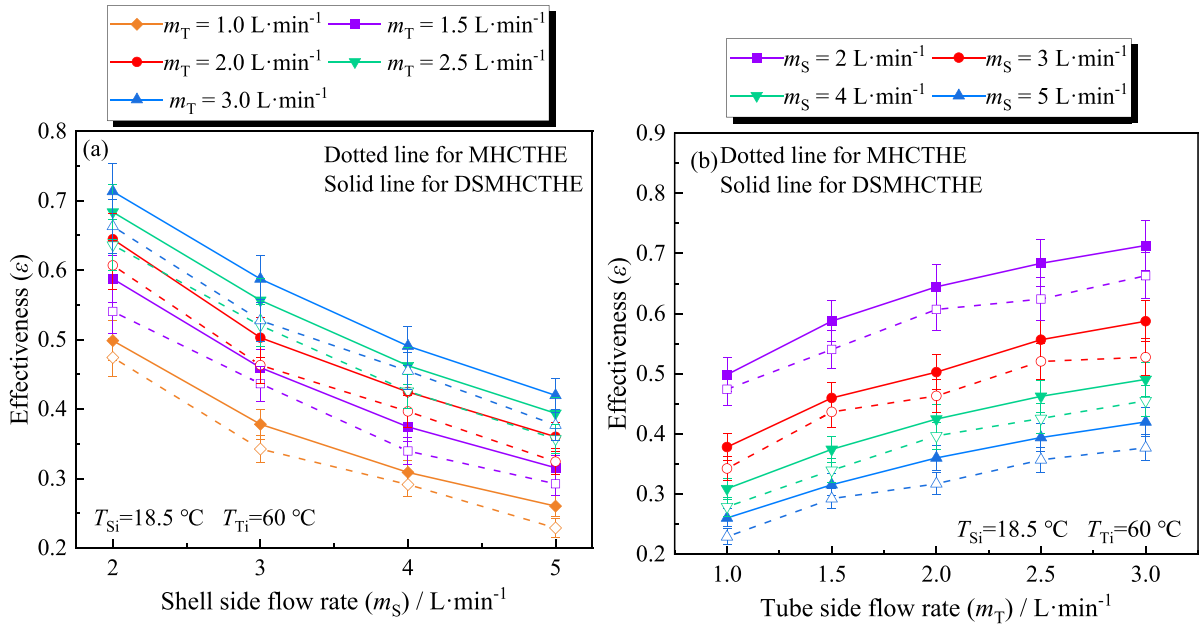

Fig. 16. Variation of heat transfer effectiveness with flow rate of the heat exchangers.

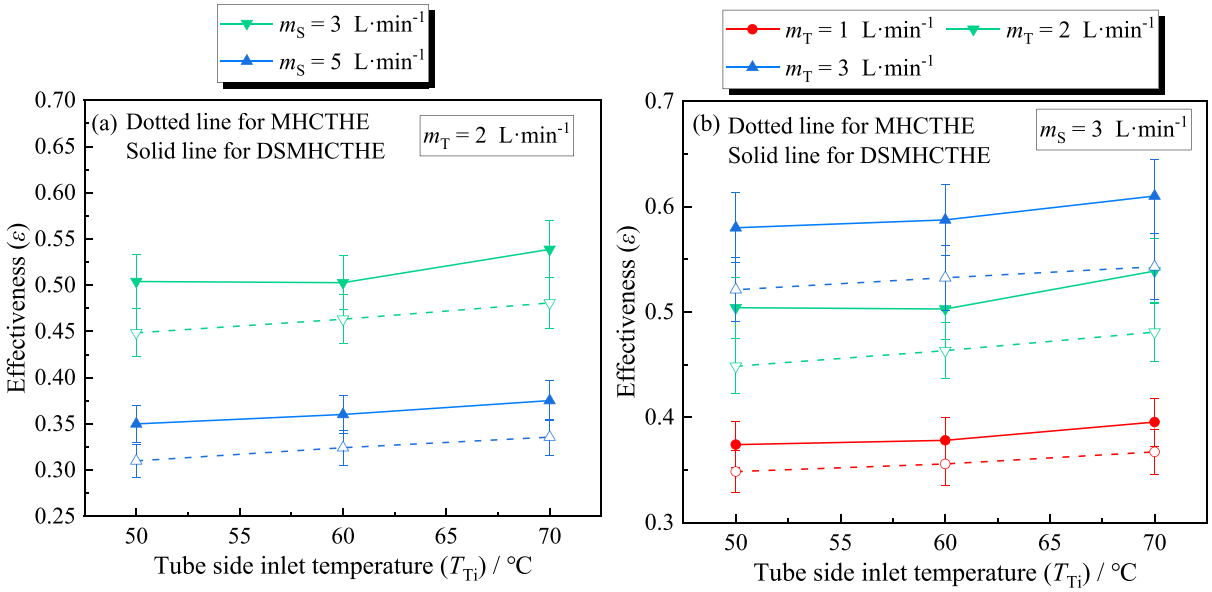

Fig. 17. Variation of heat transfer effectiveness with inlet temperature difference of the heat exchangers.

Table 5
Comparison of this work with literatures on similar helically coiled tube heat exchangers.

	Method		Flow rate of shell-side	Flow rate of tube-side	Q (W)	h_S (W·m^{-2}·K^{-1})	h_T (W·m^{-2}·K^{-1})	U_o (W·m^{-2}·K^{-})
	Exp	Sim						
Shokouhmand[7]	√		0.019–0.136 kg·s^{-1}	0.016–0.113 kg·s^{-1}	—	—	1467–4267	270–700
Alper[29]	√	√	2–6 L·min^{-1}	3–4 L·min^{-1}	2950–5350	1090–2700	5200–6500	800–1400
Salem[35]	√		1.7–11.2 L·min^{-1}	1.7–11.2 L·min^{-1}	—	—	—	200–1500
Tuncer[36]	√	√	2–3 L·min^{-1}	0.031–0.076 kg·s^{-1}	2000–4600	2250–4050	5700–13,400	1600–3150
Panahi[34]	√		1–5 L·min^{-1}	1–3 L·min^{-1}	—	—	—	475–1700
Miansari[27]		√	0.015–0.66 kg·s^{-1}	0.03 kg·s^{-1}	1773–3069	—	—	—
Wang[37]		√	0.5–1.5 L·min^{-1}	0.5–1.5 L·min^{-1}	1000–1650	—	—	—
Jamshidi[9]	√		1–4 L·min^{-1}	1–4 L·min^{-1}	—	—	—	475–1143
Ghorbani[12]	√		0.03–0.113 kg·s^{-1}	0.03–0.113 kg·s^{-1}	1538–13,513	480–1520	—	405–1200
MHCTHE	√	√	**2–5 L·min^{-1}**	**2–6 L·min^{-1}**	**2700–6039**	**794–1366**	**2450–6590**	**569–976**
DSMHCTHE	√	√	**2–5 L·min^{-1}**	**2–6 L·min^{-1}**	**2900–6750**	**1135–1963**	**2450–6590**	**724–1247**

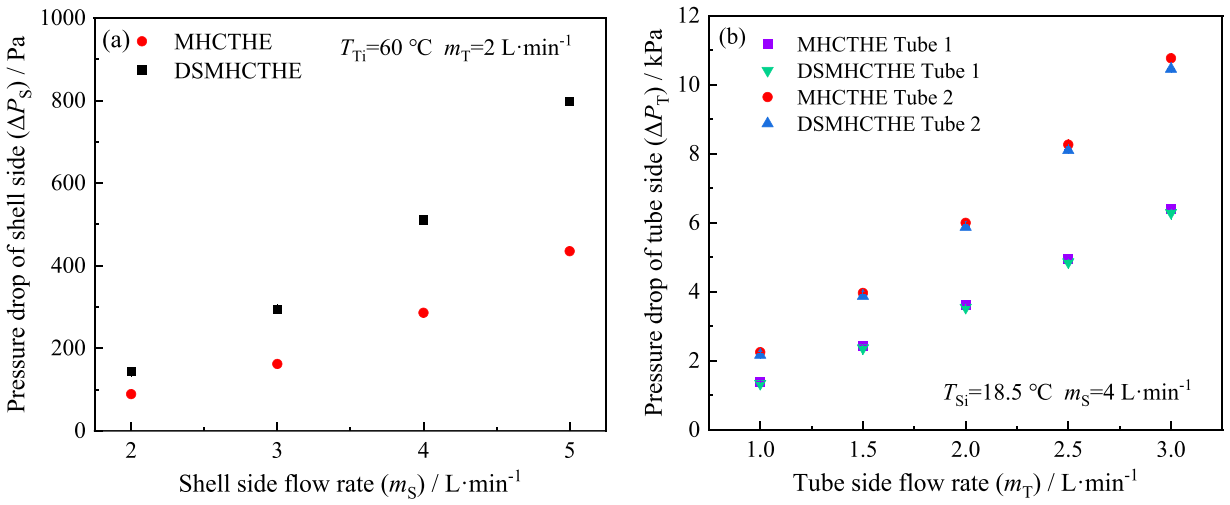

Fig. 18. Variation of pressure drop on both sides of the heat exchangers.

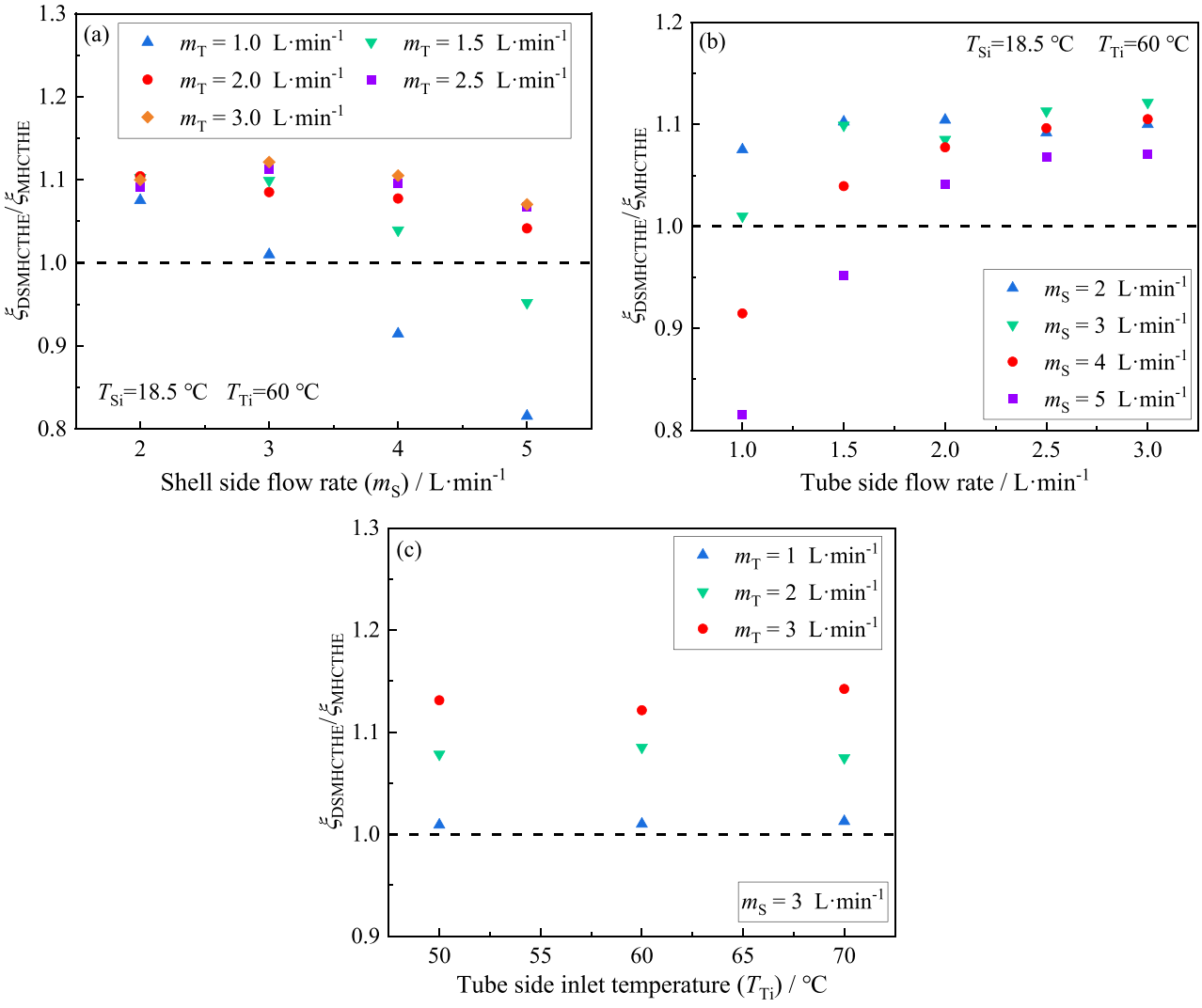

Fig. 19. Changes in the ratio of comprehensive performance of the heat exchangers.

6. Conclusion

This study proposes a novel double shell-passes structure for a multi-layer helically coiled tubes heat exchanger (DSMHCTHE) to enhance the heat transfer performance of the shell-side in helically coiled tube heat exchangers. The performance of DSMHCTHE is investigated through numerical simulations, and a comparison is made with a conventional multi-layer helically coiled tubes heat exchanger (MHCTHE).

Furthermore, physical models of both heat exchangers are fabricated, and an experimental test system is established to study their performance. The variations in heat transfer, resistance, and comprehensive performance of the two heat exchangers under different flow rates and inlet temperatures are explored.

The results indicate that the proposed double shell-passes structure design significantly improves the performance, with DSMHCTHE exhibiting superior heat transfer performance compared to MHCTHE, albeit with a higher shell-side pressure drop. Under the same experimental conditions, the heat transfer rate and thermal effectiveness of DSMHCTHE increased by 5.1 % to 12.9 %, the overall heat transfer coefficient increased by 21.5 % to 29.0 %, the shell-side heat transfer coefficient increased by 36.2 % to 47.5 %, and the shell-side pressure drop increased by 60.7 % to 83.4 %. Additionally, using the heat exchanger's comprehensive performance as an evaluation criterion, DSMHCTHE demonstrates superior comprehensive performance. Compared to MHCTHE, DSMHCTHE's comprehensive performance improves by 12 %.

CRediT authorship contribution statement

Yuyang Yuan: Writing – original draft, Visualization, Validation, Software, Methodology, Investigation, Formal analysis, Data curation. **Jiaming Cao:** Writing – review & editing, Validation, Software, Investigation. **Zhao Zhang:** Writing – review & editing, Software, Data curation. **Zhengyan Xiao:** Writing – review & editing, Investigation, Data curation. **Xuesheng Wang:** Writing – review & editing, Supervision, Methodology.

Declaration of competing interest

We declare that we have no financial and personal relationships with other people or organizations that can inappropriately influence our work.

Data availability

Data will be made available on request.

References

[1] P. Sahoo, M.I. Ansari, A. Datta, A computer based iterative solution for accurate estimation of heat transfer coefficients in a helical tube heat exchanger [J], J. Food Eng. 58 (3) (2003) 211–214.

[2] D.G. Prabhanjan, T.J. Rennie, G.V Raghavan, Natural convection heat transfer from helical coiled tubes [J], Int. J. Therm. Sci. 43 (4) (2004) 359–365.

[3] S. Hashemi, M. Akhavan-Behabadi, An empirical study on heat transfer and pressure drop characteristics of CuO–base oil nanofluid flow in a horizontal helically coiled tube under constant heat flux [J], Int. Commun. Heat Mass Transf. 39 (1) (2012) 144–151.

[4] B. Bhanvase, S. Sayankar, A. Kapre, et al., Experimental investigation on intensified convective heat transfer coefficient of water based PANI nanofluid in vertical helical coiled heat exchanger [J], Appl. Therm. Eng. 128 (2018) 134–140.

[5] S. Rainieri, F. Bozzoli, L. Cattani, et al., Compound convective heat transfer enhancement in helically coiled wall corrugated tubes [J], Int. J. Heat. Mass Transf. 59 (2013) 353–362.

[6] H. ITO, Friction Factors for Turbulent Flow in Curved Pipes [J], J. Basic Eng. 81 (2) (1959) 123–132.

[7] H. Shokouhmand, M.R. Salimpour, M.A Akhavan-Behabadi, Experimental investigation of shell and coiled tube heat exchangers using wilson plots [J], Int. Commun. Heat Mass Transf. 35 (1) (2008) 84–92.

[8] M.R. Salimpour, Heat transfer coefficients of shell and coiled tube heat exchangers [J], Exp. Therm. Fluid. Sci. 33 (2) (2009) 203–207.

[9] N. Jamshidi, M. Farhadi, D.D. Ganji, et al., Experimental analysis of heat transfer enhancement in shell and helical tube heat exchangers [J], Appl. Therm. Eng. 51 (1–2) (2013) 644–652.

[10] G. Taguchi, Taguchi techniques for quality engineering [J], Q. Resour., New York (1987) 253–255.

[11] M. Majid Etghani, S. Amir Hosseini Baboli, Numerical investigation and optimization of heat transfer and exergy loss in shell and helical tube heat exchanger [J], Appl. Therm. Eng. 121 (2017) 294–301.

[12] N. Ghorbani, H. Taherian, M. Gorji, et al., Experimental study of mixed convection heat transfer in vertical helically coiled tube heat exchangers [J], Exp. Therm. Fluid. Sci. 34 (7) (2010) 900–905.

[13] N. Ghorbani, H. Taherian, M. Gorji, et al., An experimental study of thermal performance of shell-and-coil heat exchangers [J], Int. Commun. Heat Mass Transf. 37 (7) (2010) 775–781.

[14] Y. Yuan, J. Cao, X. Wang, et al., Economic-effectiveness analysis of micro-fins helically coiled tube heat exchanger and optimization based on multi-objective differential evolution algorithm [J], Appl. Therm. Eng. 201 (2022) 117764.

[15] J.C. Kurnia, A.P. Sasmito, T. Shamim, et al., Numerical investigation of heat transfer and entropy generation of laminar flow in helical tubes with various cross sections [J], Appl. Therm. Eng. 102 (2016) 849–860.

[16] M. Omidi, M. Farhadi, A.A.R Darzi, Numerical study of heat transfer on using lobed cross sections in helical coil heat exchangers: effect of physical and geometrical parameters [J], Energy Conver. Manage. 176 (2018) 236–245.

[17] L. Zheng, Y. Xie, D. Zhang, Numerical investigation on heat transfer and flow characteristics in helically coiled mini-tubes equipped with dimples [J], Int. J. Heat. Mass Transf. 126 (2018) 544–570.

[18] S. Chang, P.-S. Wu, W. Cai, et al., Turbulent flow and heat transfer of helical coils with twisted section [J], Appl. Therm. Eng. 180 (2020) 115919.

[19] G. Wang, D. Wang, X. Peng, et al., Experimental and numerical study on heat transfer and flow characteristics in the shell side of helically coiled trilobal tube heat exchanger [J], Appl. Therm. Eng. 149 (2019) 772–787.

[20] E.P. Kumar, A.K. Solanki, M.M.J Kumar, Numerical investigation of heat transfer and pressure drop characteristics in the micro-fin helically coiled tubes [J], Appl. Therm. Eng. 182 (2021) 116093.

[21] H. Barzegari, A. Tavakoli, D. Jalali Vahid, et al., Experimental study of heat transfer enhancement in a helical tube heat exchanger by alumina nanofluid as current flow [J], Heat. Mass Transf. 55 (2019) 2679–2688.

[22] A.F. Niwalkar, J.M. Kshirsagar, K. Kulkarni, Experimental investigation of heat transfer enhancement in shell and helically coiled tube heat exchanger using SiO2/water nanofluids [J], Mater. Today: Proc. 18 (2019) 947–962.

[23] M. Zaboli, S. Saedodin, S.S. Mousavi Ajarostaghi, et al., Numerical evaluation of the heat transfer in a shell and corrugated coil tube heat exchanger with three various water-based nanofluids [J], Heat Transf. 50 (6) (2021) 6043–6067.

[24] A.S. Baqir, H.B. Mahood, A.R Kareem, Optimisation and evaluation of NTU and effectiveness of a helical coil tube heat exchanger with air injection [J], Therm. Sci. Eng. Prog. 14 (2019) 100420.

[25] H. Sadighi Dizaji, S. Jafarmadar, M. Abbasalizadeh, et al., Experiments on air bubbles injection into a vertical shell and coiled tube heat exchanger; exergy and NTU analysis [J], Energy Conver. Manage. 103 (2015) 973–980.

[26] S. Khorasani, A. Dadvand, Effect of air bubble injection on the performance of a horizontal helical shell and coiled tube heat exchanger: an experimental study [J], Appl. Therm. Eng. 111 (2017) 676–683.

[27] M. Miansari, M.A. Valipour, H. Arasteh, et al., Energy and exergy analysis and optimization of helically grooved shell and tube heat exchangers by using Taguchi experimental design [J], J. Therm. Anal. Calorim. 139 (2020) 3151–3164.

[28] R. Andrzejczyk, T. Muszynski, Thermodynamic and geometrical characteristics of mixed convection heat transfer in the shell and coil tube heat exchanger with baffles [J], Appl. Therm. Eng. 121 (2017) 115–125.

[29] G. Alper, K. Ataollah, S. Adnan, et al., Numerical and experimental study on thermal performance of a novel shell and helically coiled tube heat exchanger design with integrated rings and discs [J], Int. J. Therm. Sci. 182 (2022) 107781.

[30] B.E. Launder, D.B Spalding, Lectures in Mathematical Models of Turbulence [M], Academic Press, London, 1972.

[31] T. Wenquan, Numerical heat transfer [M]. Shanxi: Xi'An Jiao Tong University Publishing Company, 2001.

[32] R.L. Manlapaz, S.W Churchill, Fully developed laminar convection from a helical coil [J], Chem. Eng. Commun. 9 (1–6) (1981) 185–200.

[33] G. Rogers, Y Mayhew, Heat transfer and pressure loss in helically coiled tubes with turbulent flow [J], Int. J. Heat. Mass Transf. 7 (11) (1964) 1207–1216.

[34] D. Panahi, K. Zamzamian, Heat transfer enhancement of shell-and-coiled tube heat exchanger utilizing helical wire turbulator [J], Appl. Therm. Eng. 115 (2017) 607–615.

[35] M. Salem, K. Elshazly, R. Sakr, et al., Experimental investigation of coil curvature effect on heat transfer and pressure drop characteristics of shell and coil heat exchanger [J], J. Therm. Sci. Eng. Appl. 7 (1) (2015) 011005.

[36] A.D. Tuncer, A. Sözen, A. Khanlari, et al., Analysis of thermal performance of an improved shell and helically coiled heat exchanger [J], Appl. Therm. Eng. 184 (2021) 116272.

[37] C. Wang, Z. Cui, H. Yu, et al., Intelligent optimization design of shell and helically coiled tube heat exchanger based on genetic algorithm [J], Int. J. Heat. Mass Transf. 159 (2020) 120140.